Interaction induced effects in the nonlinear Raman response of liquid CS2

la Cour Jansen, T.; Snijders, J. G.; Duppen, K.

Published in:
Journal of Chemical Physics

DOI:
10.1063/1.1374959

Publication date:
2001

Interaction induced effects in the nonlinear Raman response of liquid CS_2: A finite field nonequilibrium molecular dynamics approach

Thomas I. C. Jansen, Jaap G. Snijders, and Koos Duppen

Citation: J. Chem. Phys. **114**, 10910 (2001); doi: 10.1063/1.1374959
View online: https://doi.org/10.1063/1.1374959
View Table of Contents: http://aip.scitation.org/toc/jcp/114/24
Published by the American Institute of Physics

Interaction induced effects in the nonlinear Raman response of liquid CS_2: A finite field nonequilibrium molecular dynamics approach

Thomas I. C. Jansen and Jaap G. Snijders
Theoretical Chemistry, Materials Science Centre, Rijksuniversiteit Groningen (RuG), Nijenborgh 4, 9747 AG Groningen, The Netherlands

Koos Duppen
Ultrafast Laser Laboratory, Materials Science Centre, Rijksuniversiteit Groningen (RuG), Nijenborgh 4, 9747 AG Groningen, The Netherlands

(Received 8 December 2000; accepted 5 April 2001)

The third- and fifth-order time-domain Raman responses of liquid carbon disulfide have been calculated, taking local field effects into account through the dipole-induced dipole approximation to the polarizability. The third-order response is shown to be in excellent agreement with experimental data. The calculated two-dimensional shape of the fifth-order response is compared with recently reported experimental observations of what is claimed to be pure fifth-order response. Considerable discrepancies are observed which might be explained by contamination of the experimental results with sequential and especially parallel third-order cascaded Raman response. A new choice of polarization conditions is proposed, which increases the discrimination against these unwanted cascading effects, as compared to the previously discussed fully polarized and magic angle conditions. © *2001 American Institute of Physics.* [DOI: 10.1063/1.1374959]

I. INTRODUCTION

The ultrafast dynamics in liquids can be studied by femtosecond laser spectroscopy techniques. Examples of such experiments are the (heterodyned) optical Kerr effect[1,2] and transient grating scattering.[3,4] The advantage of these methods, that are examples of time-resolved stimulated Raman scattering experiments, is that they make it possible to observe the induced motions in real time, rather than as resonance. Despite this advantage, the information content in such time domain experiments is in principle the same as in frequency domain light scattering experiments. The two types of experiments are related by Fourier transforms.

Tanimura and Mukamel suggested the use of two-dimensional Raman spectroscopy[5] to give a more detailed understanding of liquid dynamics. In these experiments two Raman perturbations, separated by a time of free evolution, are applied to the sample. After another period of free evolution the state of the sample is probed. This kind of experiment can be expected to give much more information on the structural dynamics of the liquid than the one-dimensional experiments. For instance, the two-dimensional data contain information on whether the broadening of the Raman spectrum is dominated by ultrafast fluctuations on a local molecular scale or by density fluctuations on a much larger length scale.[5,6] The line broadening mechanisms are in the limiting cases described as homogeneous line broadening, due to interaction of the system with a fast heat bath, and inhomogeneous line broadening, from a slowly fluctuating distribution of local environments. The two-dimensional data also contain information about mode coupling effects, comparable to the well-known coupling effects between spins in two-dimensional nuclear magnetic resonance (NMR).[7,8]

Concepts like homogeneous and inhomogeneous line broadening are based on abstract models with an unclear physical interpretation. Brownian oscillator models[6,9] are more detailed but still abstract and difficult to interpret. Predictions of intensities and intensity ratios between the fifth-order response and the third-order cascaded processes cannot be made from these models, since the third- and fifth-order responses are dominated by different parts of a Taylor expansion of the susceptibility in the coordinates. To provide even a basic understanding of the high-order Raman experiments and interpret the results in terms of physical relevant information on liquids, more microscopic models are required.

Molecular dynamics (MD) simulations can provide the microscopic information needed to give spectral predictions and provide the understanding of the underlying physics. The instantaneous normal modes (INM) method[10–13] uses snapshots of the potential surface from molecular dynamics simulations, to describe the molecular motion that gives rise to the Raman spectrum. The use of instantaneous snapshots limits this method to the description of phenomena on a very short time scale and the method therefore is not able to describe properties such as diffusive motion. From full molecular dynamics simulation data, the nonlinear Raman spectra can be predicted using classical time correlation functions (TCF).[14–18] This provides good possibilities to calculate the third-order response function, but the approach is not well suited for higher-order response, since the time correlation functions related to the higher-order response become too complicated to calculate from the numerical MD data.[19] Alternatively, a nonequilibrium MD method, where the actual experiment is simulated by applying laser fields during the simulations, can be used. This finite field (FF) method[20] makes it possible to calculate the fifth-order response in a way that is numerically much less expensive. The third-order response has also been modeled using a quasicrystal

model[21,22] in which the molecular movements are approximated by the motion in short lived quasicrystalline structures.

The third- and fifth-order responses were calculated earlier by us neglecting the many-body part of the optical response.[20] In this model the polarizability of the sample is calculated as the sum of single molecule contributions. The calculated third-order response showed good agreement with experiment in the diffusive tail, but serious discrepancies occurred in the short time response. These discrepancies were attributed to the fact that interaction induced effects were not taken into account in the calculation of the polarizability. The intensity ratios found between the fifth-order and the third-order cascaded response supported the conclusion that the experimentally observed fifth-order spectra[23–25] were highly dominated by cascading third-order processes.[26] Very recently new sets of experiments with improved measuring conditions have been reported.[27,28] The results of Blank *et al.*[27] could not be explained by cascaded response alone and therefore it was concluded that the true fifth-order response was measured. The experiments by Astinov *et al.*[28] showed a weak nuclear fifth-order response.

In this paper, the fifth-order optical response of liquid CS_2 is calculated, taking many-body effects in the optical interactions into account. The outline is as follows: In Sec. II it will be described how the nonlinear Raman response can be calculated, with emphasis on the finite field method. A way to estimate the intensity ratio between the true fifth-order response and the competing third-order cascading processes will be given. In Sec. III it is described how local field effects can be taken into account through the dipole-induced dipole (DID) model. Then, in Sec. IV the third-order response, calculated with different methods will be presented and compared with experimental data. Next, the two-dimensional fifth-order response is also calculated and compared with the most recent experimental data.[27] In Sec. V the main conclusions of this paper are presented.

II. NONLINEAR RAMAN RESPONSE

In a time-domain one-dimensional Raman experiment an initial laser pulse pair perturbs the sample and after a delay t_1 the dynamics, following the impact of the initial pulse pair is probed by a third laser pulse. This is shown in Fig. 1. The signal is governed by the third-order response function $\chi^{(3)}_{abcd}$, where *b*, *c*, and *d* are the polarization directions of the driving fields and *a* is the polarization direction of the emitted Rayleigh/Raman radiation. The possible polarization directions for the nuclear third-order response are limited by symmetry.[29] Because the liquid phase is isotropic, the only tensor elements of the polarization with nonzero response are $\chi^{(3)}_{zzzz}$, $\chi^{(3)}_{zzxx}$, $\chi^{(3)}_{zxzx}$, and $\chi^{(3)}_{zxxz}$. All permutations of *x*, *y*, and *z* and linear combinations of these response functions are possible. The four response functions are not linearly independent but are related by two expressions,[29]

$$\chi^{(3)}_{zxxz}(t)=\chi^{(3)}_{zxzx}(t),$$
$$\chi^{(3)}_{zzxx}(t)=\chi^{(3)}_{zzzz}(t)-2\chi^{(3)}_{zxzx}(t). \tag{1}$$

Hence, finding two of these response functions will provide all the information we can obtain. Usually $\chi^{(3)}_{zzzz}$ and $\chi^{(3)}_{zxzx}$ are the functions determined experimentally. They are denoted as the polarized and the depolarized components of the response. Alternatively a separation into a part due to fluctuations of the anisotropic part of the susceptibility and another due to fluctuations of the isotropic part of the susceptibility can be used. The depolarized component and the anisotropic response are identical. The linear combination with equal weight of $\chi^{(3)}_{zzxx}$, $\chi^{(3)}_{zzyy}$, and $\chi^{(3)}_{zzzz}$ is equivalent with the response function $\chi^{(3)}_{zzmm}$, where *m* denotes an axis forming an angle of 54.74° with the *z* axis (the magic angle). This tensor element contains only information about the fluctuations of the isotropic part of the susceptibility. In the independent molecule model of the susceptibility, it vanishes because the isotropic susceptibility in the model is constant.

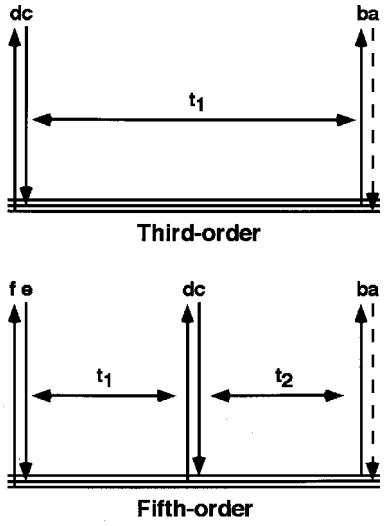

FIG. 1. Energy level diagrams for the third- and fifth-order Raman responses. The full arrows symbolizes the driving fields and the dashed arrows the emitted field. The polarization directions (*a*, *b*, *c*, *d*, *e*, and *f*) of the fields are shown above the arrows.

Any response component $\chi^{(3)}_{zzkk}$, where *k* denotes an axis forming an angle of θ degrees, with the *z*-axis, can be expressed as[29]

$$\chi^{(3)}_{zzkk}=\cos^2\theta\times\chi^{(3)}_{zzzz}+\sin^2\theta\times\chi^{(3)}_{zzyy}. \tag{2}$$

Later a choice of θ at 60° will be considered. The axis connected with this angle, close to the magic angle, will be denoted with an *l*. It should be realized that an angle of 120° gives the exact same response as with 60°. It will be shown later that this can effectively be used to suppress the cascaded response. In Fig. 2 the polarization directions of the $\chi^{(3)}_{zzzz}$ and $\chi^{(3)}_{zzll}$ components are illustrated.

In the time-domain two-dimensional Raman experiment two initial laser pulse pairs with an intermediate time delay t_1 are followed by a Raman probe pulse after an additional time delay t_2 as illustrated in Fig. 1. The two-dimensional signal is governed by the fifth-order response function $\chi^{(5)}_{abcdef}$, where *b*, *c*, *d*, *e*, and *f* are the polarization directions of the driving fields and *a* is the polarization direction of the measured signal. For the nuclear fifth-order response similar symmetry considerations hold as those made for the third-order response and there are five linearly independent tensor

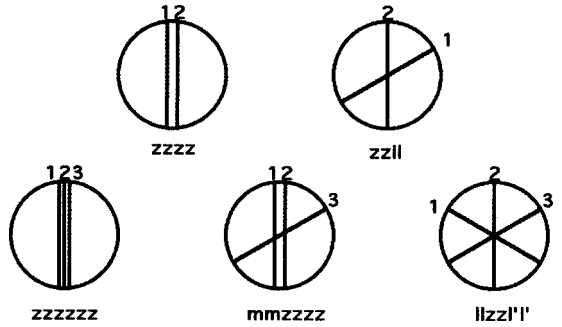

FIG. 2. In the upper line the polarization directions of the $\chi^{(3)}_{zzzz}$ and $\chi^{(3)}_{zzll}$ tensor components are illustrated. The circle is the unit circle in the plane perpendicular to the propagation direction of the laser beams. The lines symbolizes the polarization alignment of the pulse pairs and the probe and signal fields. Since the pulses in the considered experiments come in aligned pairs and the Raman events depend on the product of the aligned fields, the orientation of the polarization vector of each field is not important. In the third-order case line 1 is the driving field pulse pair and line 2 is the probe and signal fields. In the lower line the polarization directions of the fifth-order tensor components $\chi^{(5)}_{zzzzzz}$, $\chi^{(5)}_{mmzzzz}$, and $\chi^{(5)}_{llzzl'l'}$ are illustrated. Line 1 and 2 are driving field pulse pairs and line 3 is the probe and signal fields.

elements.[30] Here, the tensor elements $\chi^{(5)}_{zzzzzz}$, $\chi^{(5)}_{zzzzmm}$, $\chi^{(5)}_{zzmmzz}$, and $\chi^{(5)}_{mmzzzz}$ will be discussed. The first two were recently claimed to have been measured experimentally.[27] In addition, the tensor element $\chi^{(5)}_{llzzl'l'}$ will be discussed because it is expected to suppress the cascaded response, as will be explained later. Here l denotes an angle of 60° clockwise of the z-axis seen from the direction of the incoming laser beams and l' denotes an angle of 60° counterclockwise. Thus, the angle between these two axes is 120°. The $\chi^{(5)}_{llzzl'l'}$ component is, using the expression for angle polarization direction dependence in near colinear experiments,[30] given by

$$\chi^{(5)}_{llzzl'l'}=\tfrac{3}{8}(\chi^{(5)}_{yyzzzz}+\chi^{(5)}_{zzyyzz}+\chi^{(5)}_{zzzzyy})-\tfrac{1}{8}\chi^{(5)}_{zzzzzz}. \tag{3}$$

The polarization directions of the $\chi^{(5)}_{zzzzzz}$, $\chi^{(5)}_{mmzzzz}$, and $\chi^{(5)}_{llzzl'l'}$ components are illustrated in Fig. 2.

All third- and fifth-order tensor elements can be expressed in terms of time correlation functions (TCFs). The third-order response function that governs the one-dimensional experiment, is given by the TCF of the first-order electronic susceptibility $\chi^{(1)}$, and its time derivative,[14,18,31]

$$\chi^{(3)}_{abcd}(t)=-\frac{1}{2k_bT}\langle\dot{\chi}^{(1)}_{ab}(t)\chi^{(1)}_{cd}(0)\rangle. \tag{4}$$

The time correlation function can be calculated using Brownian oscillator models,[6,9] instantaneous normal mode data (INM) from snapshots in molecular dynamics simulations[10–13] or full molecular dynamics (MD) trajectories[14–18] of the molecular motion in the sample.

Alternatively, the third-order response function can be calculated using the finite field method (FF),[20] where the actual experiment is simulated using molecular dynamics. Here the forces, due to the optical fields at time zero, are actually applied in the simulation and the response is measured by calculating the susceptibility at later time steps. This procedure is repeated for numerous trajectories to produce sufficient statistical material. Additionally the noisy background response from calculations without the applied forces, is subtracted to improve the accuracy. This approach has also been used in our earlier calculations that did not take the local field effects into account.[20] It can be easily generalized to calculations that include these effects.

Thus, the third-order response function is calculated from the difference between the susceptibility in the calculation, where electric fields E_c and E_d, are applied in a time step of duration Δt and the background calculation, where no fields are applied. The *ab* tensor element of the susceptibility, calculated with applied pump fields with polarization directions c and d, is denoted $\chi^{(1)}_{ab;cd}$, while the same tensor element from the background calculation is denoted $\chi^{(1)}_{ab;00}$. The third-order response function in a sample with number density N, is then given by

$$\chi^{(3)}_{abcd}(t)=\frac{\chi^{(1)}_{ab;cd}(t)-\chi^{(1)}_{ab;00}(t)}{4\pi\varepsilon_0 NE_cE_d\Delta t}. \tag{5}$$

The fifth-order response function governing the two-dimensional experiment is given by a time correlation function of the first-order susceptibilities that includes a Poisson bracket. This complicates the evaluation dramatically,[11,19,20,32]

$$\chi^{(5)}_{abcdef}(t_1,t_2)=\left(\frac{1}{k_BT}\right)^2\langle\chi^{(1)}_{ab}(t_1+t_2)\dot{\chi}^{(1)}_{cd}(t_1)\dot{\chi}^{(1)}_{ef}(0)\rangle - \frac{1}{k_BT}\langle\chi^{(1)}_{ab}(t_1+t_2)\{\chi^{(1)}_{cd}(t_1),\dot{\chi}^{(1)}_{ef}(0)\}\rangle. \tag{6}$$

This time correlation function can be evaluated by approximating the molecular motion by Brownian oscillators[6] or instantaneous normal modes.[11,13] Using the full molecular dynamics trajectories[19,32] is very complicated, since it involves the calculation of the full stability matrix M, that tells how the phase space coordinates evolve after an infinitesimal change of any phase space coordinate x at an earlier time,

$$M_{kj}(t_1,0)=\left\{\frac{\partial x_k(t_1)}{\partial x_j(0)}\right\}. \tag{7}$$

The stability matrix contains the number of phase space coordinates squared. All elements of M have to be known for all times in the molecular dynamics trajectory, in order to obtain the time correlation function in Eq. (6). This makes the approach unfeasible unless the number of phase space coordinates is very limited. A study on the $\chi^{(5)}_{zzzzzz}$ response of liquid xenon using a variant of this approach with only 32 atoms has recently been published.[32]

Using the finite field method[20] the evaluation of the Poisson bracket is avoided. The fifth-order response can be calculated using the first-order susceptibilities obtained from molecular dynamics simulations where fields have been applied to simulate the experiment. The stability matrix can be transformed in such a way, that the distortion of the phase space coordinates due to the applied laser fields appears in

just one column. The finite field simulation is thus in principle equivalent to calculating only this column of the transformed stability matrix. The first-order susceptibility at any time depends on the positions q of the atoms at the particular time. The perturbing laser fields are only able to change the momentum p of the atoms during the short time interval that the optical interactions occur. The distortion of the atomic positions at time t_1 due to a change of the atomic momenta at time zero can in the limit of infinitesimal distortion be expressed using the stability matrix,

$$\Delta q_k(t_1) = \sum_j \frac{\partial q_k(t_1)}{\partial p_j(0)} \Delta p_j(0). \tag{8}$$

The changes of the momenta caused by the specific distortion can be calculated from the forces originating from the interaction with the fields,

$$\Delta p_k(0) = F_k \Delta t. \tag{9}$$

A coordinate transformation of the momentum distortion vector of the system at time zero can be performed so that only one element of the vector $\Delta p_1^T(0)$ is different from zero. This allows us to rewrite Eq. (8) in the transformed coordinates,

$$\Delta q_k^T = \frac{\partial q_k^T}{\partial p_1^T} \Delta p_1^T. \tag{10}$$

This shows that only one column of the transformed stability matrix is needed to describe the change of the positions at a later time. Furthermore, only half of this vector is required since knowledge of the change of momenta is not needed to find the susceptibility. In the finite field calculations this column is of course never explicitly calculated, since the changes of the phase space coordinates are found using molecular dynamics.

The fifth-order response can be determined from four trajectories: one background trajectory without any applied fields $\chi^{(1)}_{ab;00;00}$, a trajectory with the field applied at time zero $\chi^{(1)}_{ab;00;ef}$, a trajectory with the field applied at time t_1 $\chi^{(1)}_{ab;cd;00}$, and one with fields applied at both time zero and t_1 $\chi^{(1)}_{ab;cd;ef}$. The fifth-order response function then is

$$\chi^{(5)}_{abcdef}(t_1,t_2) = \frac{\chi^{(1)}_{ab;cd;ef} + \chi^{(1)}_{ab;00;00} - \chi^{(1)}_{ab;cd;00} - \chi^{(1)}_{ab;00;ef}}{4\pi\varepsilon_0 N E_c E_d E_e E_f (\Delta t)^2}. \tag{11}$$

This treatment can easily be generalized to higher order response functions.

In the experiment the laser light is oscillating with an optical frequency ω. In the calculations this is difficult if not impossible to simulate since the time steps are usually longer than the oscillation period of the optical fields. The laser pulses are instead modeled using a dc field, but using the polarizability at the correct optical frequency. The electric field is taken to be constant inside the simulation box. The spatial variations of the fields are taken into account when solving the Maxwell equations for the complete sample using the local response function.

Solving the Maxwell equations for the optical fields, using the third- and fifth-order susceptibility found in the simulations, makes it possible to calculate the intensity of the third and the fifth-order signals. The calculation of the microscopic response of the liquid and solving the Maxwell equations for the optical fields in the sample can be done separately as long as the simulation box is much smaller than the wavelength of the optical field. By the Maxwell equations experimental parameters as the effective sample length l and the phase mismatch Δk are introduced in these coherent nonlinear interactions. The intensities also depend implicitly on the number density N, since the first-order susceptibilities depend on the number density.

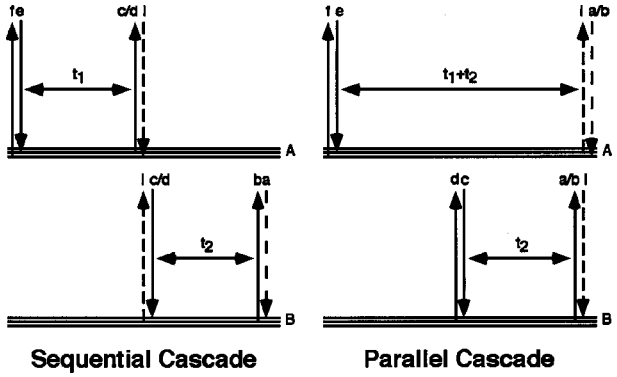

FIG. 3. Energy level diagrams for the two cascading process types. The full arrows symbolizes the driving fields that are identical to driving fields in the fifth-order response. The long-dashed arrows symbolizes the intermediate field that acts as an emitted field from one third-order process and a driving field in another third-order process. The dashed lines symbolizes the emitted field from the last third-order process. The polarization directions (a, b, c, d, e, f, and i) of the fields are shown above the arrows.

Cascading third-order processes consist of two third-order processes that are connected by an intermediate field E_i. They are induced by the same fields that give rise to the fifth-order response. The two types of cascading processes, sequential and parallel cascading, are illustrated in Fig. 3.[26] Taking the polarization direction combinations into account, two possibilities exist for each type of cascading process. The time and polarization dependence of the sequential processes of Fig. 3 are

$$\begin{aligned} \chi^{(5)}_{\mathrm{seq},1}(t_1,t_2) &= \chi^{(3)}_{abci}(t_2)\chi^{(3)}_{idef}(t_1), \\ \chi^{(5)}_{\mathrm{seq},2}(t_1,t_2) &= \chi^{(3)}_{abid}(t_2)\chi^{(3)}_{cief}(t_1). \end{aligned} \tag{12}$$

Similarly the time and polarization dependence of the two parallel cascading processes of Fig. 3 are

$$\begin{aligned} \chi^{(5)}_{\mathrm{par},1}(t_1,t_2) &= \chi^{(3)}_{aicd}(t_2)\chi^{(3)}_{ibef}(t_1+t_2), \\ \chi^{(5)}_{\mathrm{par},2}(t_1,t_2) &= \chi^{(3)}_{ibcd}(t_2)\chi^{(3)}_{aief}(t_1+t_2). \end{aligned} \tag{13}$$

Each cascading process is connected with a unique phase mismatch given by the experimental conditions. The polarization direction of the intermediate field is determined by the polarization directions of the applied fields and the polarization of the measured signal. In Table I the polarization and time dependence are given for the four components of the direct fifth-order response, considered here. There is no difference between the polarization and time dependence in the two kinds of sequential processes and the same is true for

TABLE I. In fifth-order experiments, with the polarization directions given in the first column, competing sequential and parallel cascaded processes with time and polarization dependence given in the second and third column respectively, can show up.

$\chi^{(5)}_{abcdef}$	$\chi^{(5)}_{\mathrm{seq}}$	$\chi^{(5)}_{\mathrm{par}}$
$\chi^{(5)}_{zzzzzz}$	$\chi^{(3)}_{zzzz}(t_2)\chi^{(3)}_{zzzz}(t_1)$	$\chi^{(3)}_{zzzz}(t_2)\chi^{(3)}_{zzzz}(t_1+t_2)$
$\chi^{(5)}_{mmzzzz}$	$\chi^{(3)}_{mmzz}(t_2)\chi^{(3)}_{zzzz}(t_1)$	$\chi^{(3)}_{mmzz}(t_2)\chi^{(3)}_{mmzz}(t_1+t_2)$
$\chi^{(5)}_{zzmmzz}$	$\chi^{(3)}_{mmzz}(t_2)\chi^{(3)}_{mmzz}(t_1)$	$\chi^{(3)}_{mmzz}(t_2)\chi^{(3)}_{zzzz}(t_1+t_2)$
$\chi^{(5)}_{zzzzmm}$	$\chi^{(3)}_{zzzz}(t_2)\chi^{(3)}_{mmzz}(t_1)$	$\chi^{(3)}_{zzzz}(t_2)\chi^{(3)}_{mmzz}(t_1+t_2)$
$\chi^{(5)}_{llzzl'l'}$	$\chi^{(3)}_{zzll}(t_2)\chi^{(3)}_{zzll}(t_1)$	$\chi^{(3)}_{zzll}(t_2)\chi^{(3)}_{zzll}(t_1+t_2)$

the two parallel responses. Hence, the ratio between the intensities of the true fifth-order signal and cascading processes can be of two types: sequential and parallel.

For the $\chi^{(5)}_{llzzl'l'}$ tensor component, the polarization directions of the fields in each pulse pair are parallel, but the angle between the polarization directions of the pulses in the different pairs are either 60° or 120° as illustrated in Fig. 2. Both third-order processes contributing to any cascaded signal will be given by pulse pairs with polarization directions separated by 60° or 120°. These third-order response functions are equivalent [Eq. (2)] and were denoted $\chi^{(3)}_{zzll}$. This means that both types of cascaded signals depend on the $\chi^{(3)}_{zzll}$ response squared and therefore all third-order cascaded processes are suppressed equivalently. The $\chi^{(3)}_{zzll}$ third-order component is similar to the third-order magic angle response, which is expected to be small. The crucial difference between the $\chi^{(5)}_{llzzl'l'}$ component and the magic angle components of Table I is that in the $\chi^{(5)}_{llzzl'l'}$ component the polarization direction of all three pulse pairs are separated, while in the magic angle components, discussed so far, the polarization direction of two of the pulse pairs are parallel, allowing contributions to the cascaded processes from the intensive $\chi^{(3)}_{zzzz}$ process. This is depicted in Fig. 2. In the Results, the advantage of the $\chi^{(5)}_{llzzl'l'}$ tensor element will be worked out quantitatively.

The intensity ratio between each of the third-order cascading processes and the direct fifth-order response can be estimated from the peak intensities as[20,26]

$$\frac{I_{\mathrm{cas}}}{I_{\mathrm{5th}}}=\left(\frac{\pi\omega l}{nc}\right)^2 f^2(\Delta kl)(4\pi\varepsilon_0)^2\frac{|\chi^{(3)}\chi^{(3)}|^2}{|\chi^{(5)}|^2}. \tag{14}$$

Here, the polarization dependence is omitted for simplicity and $f(\Delta kl)$ is a number smaller than one that is determined by the phase matching conditions.

Typical experimental wavelengths $2\pi c/\omega$ are 620 (Refs. 23, 25) and 800 nm.[24] Sample thicknesses $l=1-2$ mm are typically used. The refractive index n of pure CS_2 is 1.628.[33]

The intensity ratio is divided into a ratio independent of the experimental conditions R_{abcdef} that can be used for comparison between different calculations and an experimental factor that depends on the experimental conditions. The experiment independent ratio is defined as

$$R=(4\pi\varepsilon_0)^2\frac{|\chi^{(3)}\chi^{(3)}|^2}{|\chi^{(5)}|^2}, \tag{15}$$

where the polarization directions and time dependencies are given in Table I. The experimental factor F_{ex} is the part of Eq. (14) not accounted for in Eq. (15) and given by

$$F_{\mathrm{ex}}=\left(\frac{\pi\omega l}{nc}\right)^2 f^2(\Delta kl). \tag{16}$$

III. LOCAL FIELD EFFECTS

In our earlier studies[20] the first-order susceptibility $\chi^{(1)}$ was approximated by the ensemble average of the molecular polarizabilities α_n, where n is a number labeling the different molecules. The third-order response function, calculated using this approximation, showed good agreement with experiment at long times. At sub-ps times a discrepancy was found between the calculated and the experimental functions. It was speculated that interaction induced many-body effects, missing in the simple description, are crucial at sub-ps times.

Local field effects can be included in the calculation of the susceptibility by using the dipole-induced dipole correction to the electric field. An individual molecule does not only feel the macroscopic field inside the sample, but also the electric fields generated by the induced dipole moments on molecules in the local surroundings. The surroundings can be divided into two areas: the nearby surroundings with distinct local structure and the surroundings far away that can be described by a continuous dielectric medium. Here the structured surroundings will be considered to be inside a spherical cavity around the individual molecule. The electric field generated by the induced dipoles in the dielectric medium is taken into account by using the macroscopic electric field instead of the external electric field. The macroscopic field is the electric field inside a continuous dielectric sample, due to an external field, applied outside the sample in vacuum. The local electric field on each molecule arises from the macroscopic field and the induced dipole moments on the nearby molecules within the spherical cavity, which are taken into account through a dipole interaction term. The contribution from the continuous dielectric medium inside the cavity is eliminated by subtracting a term due to the polarization of a spherical dielectric medium.[31,34] This approach is depicted schematically in Fig. 4. So the local electric field on molecule n is

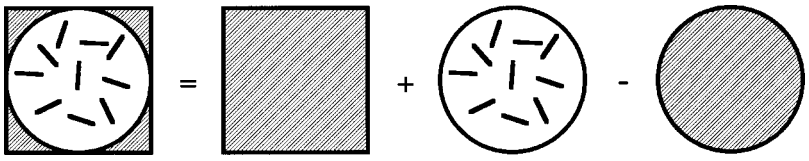

FIG. 4. The local fields acting on a molecule in a medium with local structure inside a cavity surrounded by a continuous dielectric medium can be divided into the contribution from the dielectric medium, the contribution from the molecules inside the cavity, and subtracting the dielectric medium inside the cavity.

$$E_n^{\text{local}} = E^{\text{mac}} + \sum_{m \neq n} T_{nm}\mu_m + \frac{4\pi\chi^{(1)}}{3}E^{\text{mac}}. \tag{17}$$

Here T_{nm} is the dipole tensor and μ_m is the induced dipole moment on molecule m,

$$T_{nm} = \frac{3\hat{r}_{nm}:\hat{r}_{nm} - 1}{r_{nm}^3}. \tag{18}$$

Solving a linear set of equations for the independent molecules,[14] the susceptibility can be found as well as the index of refraction and the dielectric constant. Both are related to the first-order susceptibility. An effective polarizability $\Pi_n^{(1)}$, reproducing the same induced-dipole moment from the macroscopic field as generated by polarizability α_n in the local field, is defined for simplicity,

$$\mu_n = \alpha_n E_n^{\text{local}} \equiv \Pi_n^{(1)} E^{\text{mac}}. \tag{19}$$

Combining Eqs. (17) and (19) give

$$\Pi_n^{(1)} E^{\text{mac}} = \alpha_n \left(1 + \frac{4\pi\chi^{(1)}}{3}\right) E^{\text{mac}} + \alpha_n \sum_{m \neq n} T_{nm}\Pi_m^{(1)} E^{\text{mac}}. \tag{20}$$

The first-order susceptibility is related to the effective polarizabilities through the polarization P, and the ensemble volume V, as

$$\chi^{(1)} E^{\text{mac}} = P = \frac{1}{V}\sum_n \mu_n = \frac{1}{V}\sum_n \Pi_n^{(1)} E^{\text{mac}}. \tag{21}$$

From Eq. (20) the actual macroscopic field is easily eliminated,

$$\Pi_n^{(1)} = \alpha_n \left(1 + \frac{4\pi\chi^{(1)}}{3}\right) + \alpha_n \sum_{m \neq n} T_{nm}\Pi_m^{(1)}. \tag{22}$$

The equation is multiplied with the inverse molecular polarizability and the terms containing the effective polarizability are isolated on the left-hand side of the equation. The inverse molecular polarizability of a linear molecule is given in Appendix A,

$$\alpha_n^{-1}\Pi_n^{(1)} - \sum_{m \neq n} T_{nm}\Pi_m^{(1)} = 1 + \frac{4\pi}{3}\chi^{(1)}. \tag{23}$$

Introducing Kronecker deltas the summation over m can be taken over all terms on the left side. When at the same time the index of the effective polarizability is changed from n to m, the effective polarizability can be isolated,

$$\sum_m (\alpha_n^{-1}\delta_{nm} - T_{nm}(1 - \delta_{nm}))\Pi_m^{(1)} = 1 + \frac{4\pi}{3}\chi^{(1)}. \tag{24}$$

By defining the matrix B,

$$B_{nm} \equiv \alpha_n^{-1}\delta_{nm} - T_{nm}(1 - \delta_{nm}), \tag{25}$$

and introducing the Lorentz factor L,

$$L = 1 + \frac{4\pi\chi^{(1)}}{3}, \tag{26}$$

to replace the term containing the susceptibility of the medium around the cavity, a linear set of equations for the effective polarizabilities appears,

$$\sum_m B_{nm}\Pi_m^{(1)} = L. \tag{27}$$

When this set of equations is solved, the first-order susceptibility can be found from Eq. (21). The dielectric constant ϵ_r and the index of refraction n are derived from the first-order susceptibility,

$$\varepsilon_r = 1 + 4\pi\chi^{(1)} = n^2. \tag{28}$$

In an actual calculation of the susceptibility, a system of finite size, i.e., the box used in a molecular dynamics simulation, has to be considered. The susceptibility in Eq. (24) can in principle be taken to be the calculated susceptibility. The equation can then be solved without any prior knowledge of the average susceptibility of this system. However this will introduce artifacts dependent on the number of molecules in the calculation, since the system is typically taken too small to represent the whole macroscopic body. In the case of a liquid the susceptibility is isotropic, but the susceptibility of the considered system is typically far from isotropic. Instead we use the time averaged value, which has the advantage that fluctuations due to specific instantaneous configurations are averaged out.

As an alternative to this method the effective polarizabilities can be found using an iterative scheme[18] based on Eq. (22), where i is the iteration number,

$$\Pi_n^{(1)[i+1]} = \alpha_n \left(1 + \frac{4\pi}{3}\chi^{(1)} + \frac{1}{2}\sum_{m \neq n} T_{nm}(\Pi_m^{(1)[i]} + \Pi_m^{(1)[i-1]})\right). \tag{29}$$

In this scheme the average susceptibility should also be used when subtracting the contribution from the dielectric medium inside the cavity.

The interaction energy H_{int}, between the macroscopic electric fields and a system of polarizable molecules is given as the sum of the energy of the individually induced dipoles in the macroscopic field, the energy of the individually induced dipoles in the field from all other dipoles, and the polarization energy needed to create the induced dipoles,[35]

$$H_{\text{int}} = -\sum_n E^{\text{mac}}\mu_n - \frac{1}{2}\sum_n \mu_n \left(\sum_{m \neq n} T_{nm}\mu_m + \frac{4\pi\chi^{(1)}}{3}E^{\text{mac}}\right) + \frac{1}{2}\sum_n E_n^{\text{local}}\mu_n. \tag{30}$$

Using Eq. (17) this can be written,

$$H_{\text{int}} = -\sum_n \left(E^{\text{mac}} - \frac{1}{2}(E_n^{\text{local}} - E^{\text{mac}}) + \frac{1}{2}E_n^{\text{local}}\right)\mu_n = -\frac{1}{2}\sum_n E^{\text{mac}}\mu_n. \tag{31}$$

Using the definition of the effective polarizabilities in Eq. (19), the total interaction energy of the system can be written as a sum over the energy of the effective polarizability of each molecule interacting with the macroscopic fields, E_a^{mac} and E_b^{mac},

$$H_{\mathrm{int}}^{a,b} = -\frac{1}{2}\sum_n E_a^{\mathrm{mac}} \Pi_n^{(1)} E_b^{\mathrm{mac}}. \tag{32}$$

The force $F_x^{a,b}$, in a given coordinate x due to the macroscopic fields E_a and E_b, is given by the derivative of the interaction energy of the system with respect to this coordinate,

$$F_x^{a,b} = -\frac{\partial H_{\mathrm{int}}^{a,b}}{\partial x}. \tag{33}$$

The force can then be expressed in terms of derivatives of the polarizability and the effective polarizabilities,

$$F_x^{a,b} = \frac{1}{2} E_a^{\mathrm{mac}} \sum_n \frac{\partial \Pi_n^{(1)}}{\partial x} E_b^{\mathrm{mac}}. \tag{34}$$

Considering only linear rigid molecules like CS_2 the coordinates can be divided into two types, namely center of mass and orientational ones. This simplifies the problem considerably, since the molecular polarizabilities only depend on the orientational coordinates while the dipole tensor only depends on the center of mass coordinates.

Differentiating Eq. (27) with respect to an orientational coordinate x^i on molecule i gives

$$\sum_m B_{nm} \frac{\partial \Pi_m^{(1)}}{\partial x^i} = -\frac{\partial \alpha_n^{-1}}{\partial x^i} \Pi_n^{(1)} \delta_{ni}. \tag{35}$$

Solving this set linear set of equations provides the derivative of the effective polarizabilities with respect to the orientational coordinates. The derivative of the inverse of the molecular polarizability is given in Appendix B.

Differentiating Eq. (24) with respect to a center of mass coordinate r^i on molecule i gives

$$\sum_m B_{nm} \frac{\partial \Pi_m^{(1)}}{\partial r^i} = \sum_m \frac{\partial T_{nm}}{\partial r^i} (1-\delta_{mn}) \Pi_m^{(1)}. \tag{36}$$

This linear set of equations provides the derivative of the effective polarizabilities and the first-order susceptibility with respect to a center-of-mass coordinate. The derivatives of the dipole tensors are given in Appendix B. In principle, the derivatives of the effective polarizabilities can also be found using an iterative procedure similar to the one described in Eq. (29) for the effective polarizabilities.

The importance of interaction induced effects in the response is most easily seen in the magic angle component of the third-order response. The isotropic part of the single molecule polarizability does not depend on the coordinates at all, so the contribution to the magic angle response from single non interacting molecules is zero. Hence, the intensity of the magic angle components shows the relative importance of the interaction induced effects. The comparison of the intensity of the magic angle responses with the intensity of the polarized responses thus gives an indication of the importance of the interaction induced effects and the single molecule orientational effects.

At the end of this section it should be remarked that the dipole-induced dipole model is an approximation of the full many-body problem. The higher multipole moments of the molecules can give a contribution to the local field as well. In addition, overlap of the electron clouds in close collisions influences the susceptibility in a way that cannot be taken into account by a multipole expansion. Such corrections will be treated in a subsequent paper.[36]

IV. RESULTS

For the MD simulations a modified version of GROMACS 1.6 (Ref. 37) was employed with a cubic simulation box containing 256 rigid CS_2 molecules at 1 bar pressure and 298 K, using a Berendsen thermostat.[38] An atomic Lennard-Jones force field[39] was used, which is known to give a fair description of properties as density, diffusion constant, and neutron and x-ray scattering data. The simulations were performed with 10 fs time steps. The experimental molecular polarizability for CS_2 at the optical wavelength of 514.5 nm is used. The polarizability at this wavelength is 8.95 $Å^3$ and the anisotropy is 10.05 $Å^3$.[40] Laser field pairs with field strength of 1.149 V/Å (dc) are applied during one time step for each Raman event in the finite field calculations. The DID model described in Sec. III is applied to incorporate the local field effects. The local field in this model was given in Eq. (17) and the set of equations that must be solved to find the effective polarizabilities was presented in Eq. (27).

The iterative procedure given in Eq. (29) has been used to calculate the effective polarizabilities, because it is faster than solving the linear equations. However, the linear equation approach in Eqs. (27), (35), and (36) has been used for calculation of the forces, since solving many sets of linear equations with an identical B matrix can be done effectively using LU decomposition of the B matrix followed by backsubstitution.[41] The cavity radius around each molecule is set to 50 Å, which is much larger than the side lengths of the simulation box. In principle this can introduce artifacts due to the periodic boundary conditions used in the molecular dynamics simulations. Calculations with cavity radius 14.5 Å, which is less than the side length of the simulations box, showed no significant difference from the 50 Å calculations, except for more noise. The noise in the calculations with cavity radius 14.5 Å is caused by the fact that molecules crossing the 14.5 Å border still give a significant contribution to the calculated local field that depends on their orientation. Upon crossing the border the influence of the local structure changes abruptly into a contribution from a continuous dielectric medium. Since a molecule might cross the boundary in the background calculation, but not in the calculation with the laser field applied or the other way around, noise arises when the cavity radius is small.

The isotropic first-order susceptibility in the Lorentz factor is calculated using the iterative method [Eq. (29)] assuming that the first-order susceptibility of the medium outside the cavity is the same as the first-order susceptibility of the simulation box. Taking the average over a long trajectory,

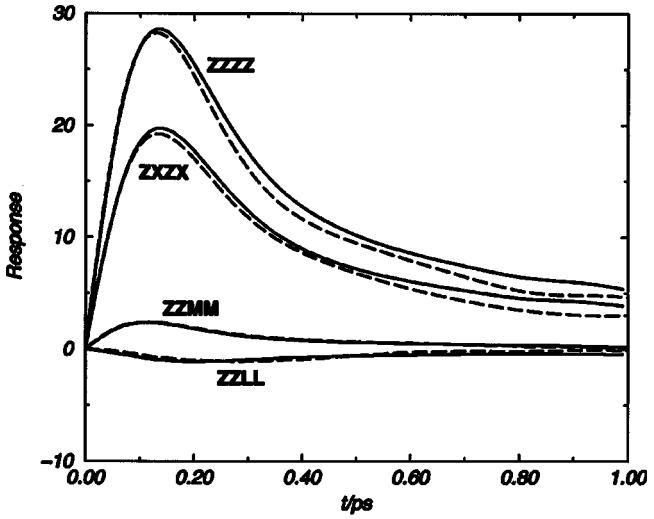

FIG. 5. The $\chi^{(3)}_{zzzz}$, $\chi^{(3)}_{zyzy}$, $\chi^{(3)}_{zzmm}$, and $\chi^{(3)}_{zzll}$ components of the third-order response given in units of $10^{-20}\,C^4\,m/J^3\,s$. The full lines are the finite field response. The dashed lines are the time correlation function response.

possible artifacts due to the assumption that the susceptibility of the simulation box is equal to the susceptibility of the whole liquid, as discussed below Eq. (28), are suppressed. From a 100 ps run a susceptibility of 0.127 85 is found, equivalent to a dielectric constant of 2.6066, a refractive index 1.6145, and a Lorentz factor 1.5355. These values are in good agreement with the experimental value of the refractive index 1.628.[33] Including the DID interaction gives a substantial improvement compared to the values found using the single molecule model of the polarizability, where we calculated a refractive index of 1.4555. Including the DID effects the error in the refractive index is thus reduced to 0.8% compared to 12% for the single molecule model. This is equivalent to a reduction of the error in the first-order susceptibility from 32% to 3%. This clearly shows how important many-body effects are in the optical response of CS_2.

The third-order TCF response was calculated from a single 10 000 ps MD simulation. The FF response was calculated from 1000 simulations of 1 ps duration and the same number of background calculations. All polarization components were obtained from the same set of trajectories. The calculated third-order response components are shown in Fig. 5 and the peak values, taken at the time when the response is most intensive, are listed in Table II. The intensities and shapes of the calculated response functions are in excellent agreement with functions reported by Kiyohara *et al.*[18] for a similar thermodynamic state, but using a slightly smaller simulation box. Very good agreement is found between the TCF and FF calculations, proving the reliability of the finite field method. The small differences are due to small statistical errors and the different nature of the calculation methods. For instance, in the TCF calculations the correlation function has to be divided by the temperature, whereas in the FF method this temperature dependence is implicitly incorporated in the molecular dynamics of the FF calculations.

The experimental $\chi^{(3)}_{zyzy}$ component provided by Steffen *et al.*[9] is compared with the finite field response with and without the DID effects in Fig. 6. Since the experiment does not provide an absolute intensity, all traces are scaled here to give the same value at 1 ps time delay. The experimental signal and the calculated response including the local field effect show excellent agreement. The response calculated without including the local field effects accounts for the long diffusive tail, but not for the intensive peak at 140 fs, which is therefore apparently dominated by local field effects. This shows that the dipole-induced dipole effect is important in the description of the response.

TABLE II. Peak values for the calculated response functions using the finite field method (FF) and the time correlation function method (TCF) when possible. Third-order values are given in units of $10^{-20}\,C^4\,m/J^3\,s$ and the fifth-order values in units of $10^{-25}\,C^6\,m^3/J^5\,s^2$. [For comparison with data in c.g.s. units: 1 e.s.u. (or cm^3) $=1.112\,64\times10^{-16}\,C^2\,m^2\,J^{-1}$, 1 erg $=10^{-7}$ J and 1 $C^4\,m/J^3\,s=8.077\,61\times10^6\,cm^3\,erg^{-1}\,ps^{-1}$.]

$\chi^{(n)}_{a\cdots b}$	FF	TCF	Deviation
$\chi^{(3)}_{zzzz}$	28.59	28.28	1.1%
$\chi^{(3)}_{mmzz}$	2.37	2.40	−1.2%
$\chi^{(3)}_{zyzy}$	19.73	19.21	2.7%
$\chi^{(3)}_{zzll}$	−1.12	−1.10	−1.8%
$\chi^{(5)}_{zzzzzz}$	0.107	⋯	⋯
$\chi^{(5)}_{mmzzzz}$	0.0327	⋯	⋯
$\chi^{(5)}_{zzmmzz}$	0.0481	⋯	⋯
$\chi^{(5)}_{zzzzmm}$	0.0346	⋯	⋯
$\chi^{(5)}_{llzzl'l'}$	−0.0252	⋯	⋯

The tail in the third-order response is usually explained as being due to single molecule realignment effects, that are well described without inclusion of the local field effects. The initial laser pulse pair exerts a torque on each molecule in a direction which is determined by the polarization direction of the fields. With inclusion of local field effects a force is exerted on the center-of-mass coordinates, as well. After a short time the excess momentum of the molecules has dissi-

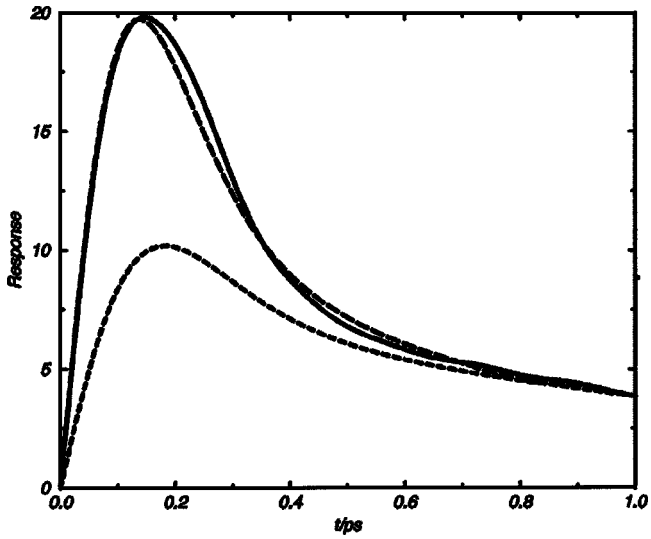

FIG. 6. The $\chi^{(3)}_{zyzy}$ component of the third-order response given in arbitrary units. The full line is the experimental response measured by Steffen *et al.* (Ref. 1) the dashed line is the finite field response, and the dotted line is the response given when the DID interaction is not included. The response functions are here scaled to give the same value at 1 ps.

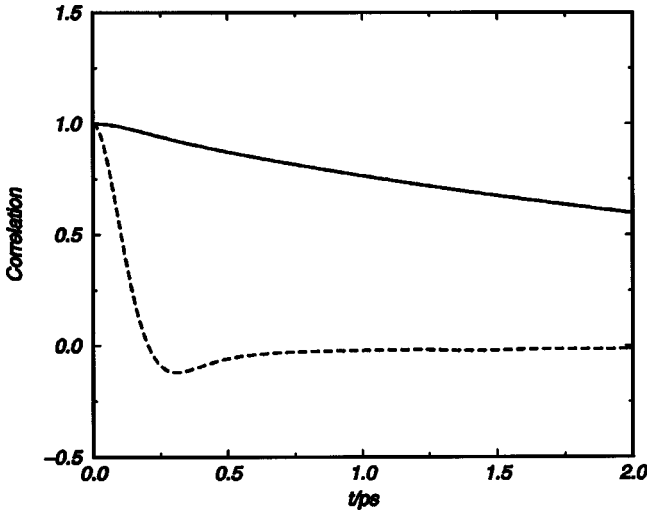

FIG. 7. The full line is the normalized orientational correlation function. The dashed line is the normalized velocity correlation function.

pated in the sense that the velocity correlation function becomes zero. The orientation of the molecules, though, is then not random yet, but still slightly aligned. Subsequently, the molecules slowly diffuse to random orientations, giving rise to a slow decay of the signal. In Fig. 7 the fast decay of the velocity correlation function and the much slower decay of the orientational correlation function, as calculated from the 10 000 ps MD run are shown. The diffusive tail is determined by the reorientation of the individual molecules and can be expected to be well described without including the interaction induced effects.

One may wonder why the magic angle component also shows this diffusive tail, since this component depends only on the fluctuations in the isotropic part of the polarizability which vanish in the independent molecule model [see discussion above Eq. (2)]. However, this can be explained by the fact that aligned molecules tend to have a higher isotropic effective polarizability than randomly oriented molecules. Hence the signal decays when the alignment is lost.

The $\chi^{(3)}_{zzmm}$ and $\chi^{(3)}_{zzll}$ responses (Fig. 5) are seen to be much less intense than the other third-order response components. $\chi^{(3)}_{zzll}$ is negative and has a maximum intensity at 200 fs, whereas the magic angle component has a maximum intensity at 110 fs. When the third-order cascaded processes, competing with the fifth-order response, contain one or preferably two of these components, the ratio of the intensities of the fifth-order signal compared to the cascaded signal is most favorable.

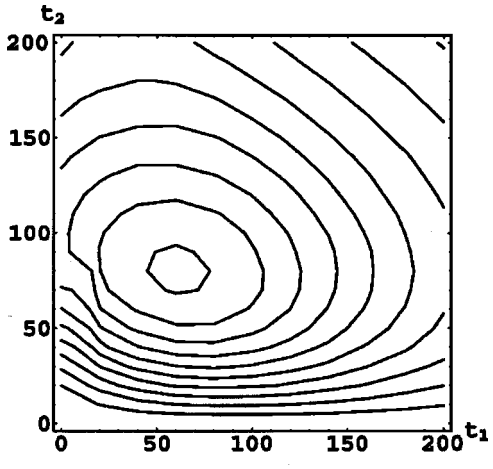

FIG. 9. The *mmzzzz* component of the fifth-order response. The time unit is fs.

The fifth-order FF response was calculated from 1000 simulations for each of the four combinations of applied laser fields shown in Eq. (11) and for t_1 values from 20 fs to 200 fs in 20 fs steps and t_2 values from 0 to 200 fs in 10 fs steps. The calculated components are obtained from two sets of trajectories giving the different polarization directions of the laser fields: one that has the polarization direction of the first laser pulse pair along the *z*-axis and one that has the polarization direction of the first laser pulse pair along the *y*-axis. The laser pulse pair applied after the delay t_1 is always applied with the polarization direction along the *z*-axis. The zz component and the yy component of the first-order susceptibility are calculated after the delay t_2. This provides the $\chi^{(5)}_{zzzzzz}$, $\chi^{(5)}_{yyzzzz}$, $\chi^{(5)}_{zzzzyy}$, and $\chi^{(5)}_{yyzzyy}$ components, from which the desired $\chi^{(5)}_{zzzzzz}$, $\chi^{(5)}_{zzzzmm}$, $\chi^{(5)}_{zzmmzz}$, $\chi^{(5)}_{mmzzzz}$, and $\chi^{(5)}_{llzzl'l'}$ tensor elements can be calculated. These are shown

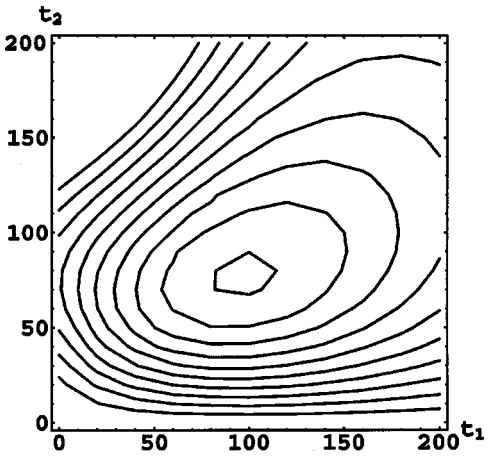

FIG. 8. The *zzzzzz* component of the fifth-order response. The time unit is fs.

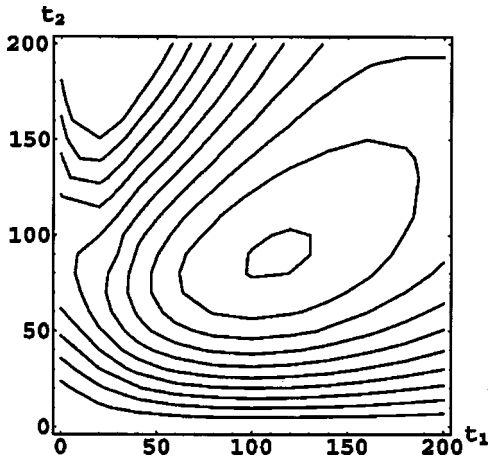

FIG. 10. The *zzmmzz* component of the fifth-order response. The time unit is fs.

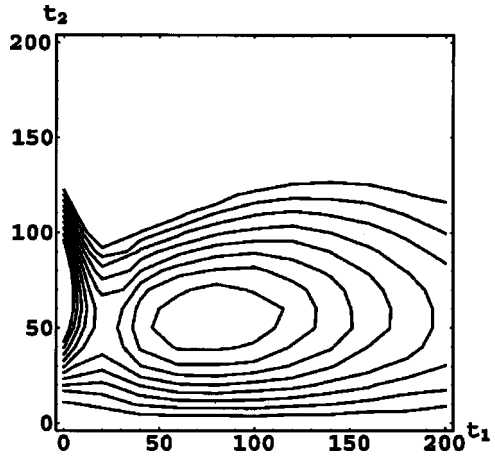

FIG. 11. The *zzzzmm* component of the fifth-order response. The time unit is fs.

in Figs. 8–12, respectively. Cuts through the surfaces along the diagonal and for t_2 fixed at 120 fs are shown for the different components in Figs. 13 and 14. In Table II the peak intensities are given and in Table III the peak positions of the cascading processes and the calculated fifth-order response are listed together with the experimental positions given by Blank *et al.*[27] Table IV contains the experiment-independent intensity ratios as defined in Eq. (15). Assuming an experimental wavelength of 620 nm, a sample length of 1 mm and perfect phase matching conditions, $f(\Delta kl)=0$, the experimental factor is 3.9×10^8 [Eq. (16)]. In the experiments performed by Blank *et al.*[27] a wavelength of 800 nm is used, which favors the true response with a factor of 1.6 in comparison with the conditions considered here.

The case least discriminating against cascaded processes is the $\chi^{(5)}_{zzzzzz}$ response, where the intensity ratio between the most intense cascaded response component and the true fifth-order response using the given experimental factor becomes 2.8×10^6 in favor of the cascading processes. In an earlier study, not including the local field effects, this ratio was found to be 4×10^6. For the magic angle component $\chi^{(5)}_{zzmmzz}$ the intensity ratio for the parallel cascaded response

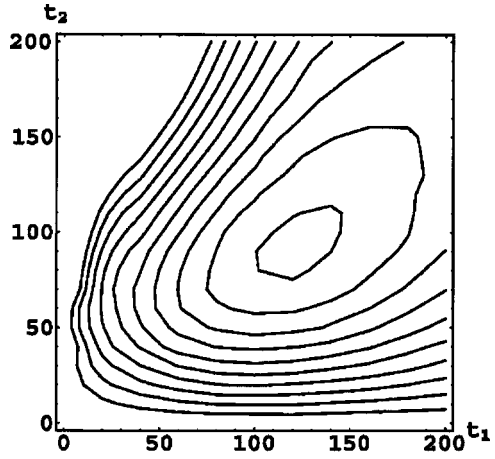

FIG. 12. The $llzzl'l'$ component of the fifth-order response. The time unit is fs.

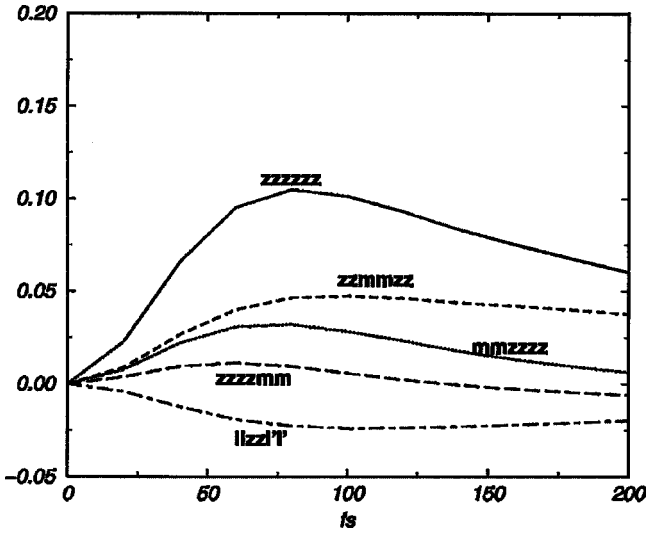

FIG. 13. Diagonal cut through the two-dimensional fifth-order response surfaces. The full line is the $\chi^{(5)}_{zzzzzz}$ component, the dotted line is the $\chi^{(5)}_{mmzzzz}$, component, the dashed line is the $\chi^{(5)}_{zzmmzz}$ component, the long dashed line is the $\chi^{(5)}_{mmzzzz}$ component, and the dashed–dotted line is the $\chi^{(5)}_{llzzl'l'}$. The response is given in units of $10^{-25}\,C^6\,m^3/J^5\,s^2$.

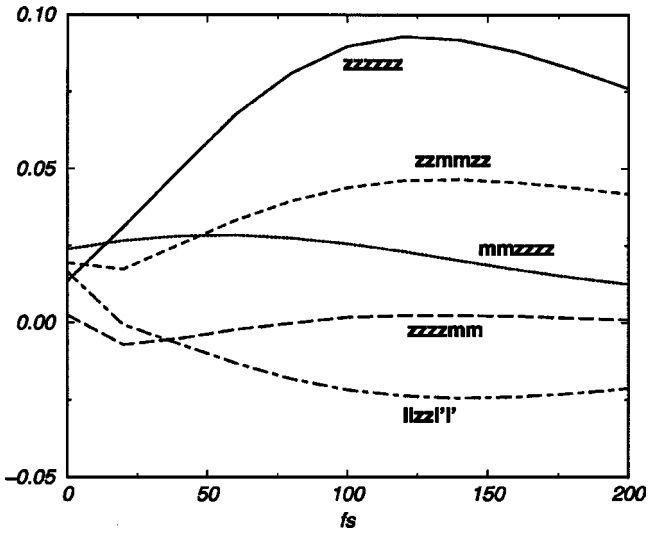

FIG. 14. Cut through the two-dimensional fifth-order response surfaces with t_2 fixed at 120 fs. The full line is the $\chi^{(5)}_{zzzzzz}$ component, the dotted line is the $\chi^{(5)}_{mmzzzz}$ component, the dashed line is the $\chi^{(5)}_{zzmmzz}$ component, the long dashed line is the $\chi^{(5)}_{mmzzzz}$ component, and the dashed–dotted line is the $\chi^{(5)}_{llzzl'l'}$ component. The response is given in units of $10^{-25}\,C^6\,m^3/J^5\,s^2$.

TABLE III. Peak positions for the direct fifth-order response and the cascading response compared with the experimental results of Blank *et al.* (Ref. 27). The peak positions are given as (t_1,t_2) in units of fs.

$\chi^{(5)}_{abcdef}$	$\chi^{(5)}_{abcdef}$	$\chi^{(5)}_{\text{seq}}$	$\chi^{(5)}_{\text{par}}$	Expt.
$\chi^{(5)}_{zzzzzz}$	(100,80)	(140,140)	(0,140)	(60,110)
$\chi^{(5)}_{mmzzzz}$	(60,80)	(140,110)	(0,110)	⋯
$\chi^{(5)}_{zzmmzz}$	(100,90)	(110,110)	(−30,110)	⋯
$\chi^{(5)}_{zzzzmm}$	(80,50)	(110,140)	(30,140)	(0,120)
$\chi^{(5)}_{llzzl'l'}$	(120,90)	(200,200)	(0,200)	⋯

TABLE IV. Experiment independent intensity ratios between the peaks of the cascaded response and the direct fifth-order response for the different polarization components.

$\chi^{(5)}_{abcdef}$	R_{seq}	R_{par}
$\chi^{(5)}_{zzzzzz}$	7.2×10^{-3}	7.2×10^{-3}
$\chi^{(5)}_{mmzzzz}$	5.3×10^{-4}	3.7×10^{-6}
$\chi^{(5)}_{zzmmzz}$	1.7×10^{-6}	2.5×10^{-4}
$\chi^{(5)}_{zzzzmm}$	4.7×10^{-4}	4.7×10^{-4}
$\chi^{(5)}_{llzzl'l'}$	3.1×10^{-7}	3.1×10^{-7}

is found to be 9.8×10^{4}. For the $\chi^{(5)}_{llzzl'l'}$ response this ratio is only 1.2×10^{2}, which allows to discriminate against the cascaded response, when the intermediate phase matching factor is better than 1×10^{3}. This is the order of magnitude reported experimentally.[27]

The fifth-order magic angle tensor elements $\chi^{(5)}_{mmzzzz}$, $\chi^{(5)}_{zzmmzz}$, and $\chi^{(5)}_{zzzzmm}$ are all approximately three times smaller than the $\chi^{(5)}_{zzzzzz}$ component. The ratio between the polarized and magic angle components in the third-order experiment is approximately 12 in favor of the polarized component. This implies that the isotropic part of the response, which cannot be explained without interaction induced effects, is much stronger in the fifth-order response than in the third-order response. The sensitivity of fifth-order response to many-body effects, found here, was recently also inferred from INM calculations by Murry *et al.*[42] This probably also means that the fifth-order signal is more sensitive to the other interaction induced effects that are described at the end of Sec. III. This is the subject of a subsequent paper.[36]

The differences between the nuclear part of the experimental signal[27] and the calculated response are pronounced. Both the $\chi^{(5)}_{zzzzzz}$ and the $\chi^{(5)}_{zzzzmm}$ component of the experimental response have sharp peaks closer to the t_2-axis than shown in the rather flat calculated two-dimensional surfaces of Figs. 8 and 11. This probably indicates that the signals are contaminated with parallel cascaded response that peaks on or close to the axis.

Comparing the calculated and experimental response is complicated by the fact that the experimental signals may include contributions from combined electronic/nuclear response along the time axes and pure electronic response for both time delays equal to zero.[6] These responses depend on the higher order nonlinear electronic responses γ and ζ, respectively. Since they are confined to the origin and the time axes, problems with separating nuclear and electronic response are limited to these areas. In addition the experimental spectra are broadened by the width of the applied laser pulses. This experimental artifact is best corrected for by deconvoluting the experimental response before comparing it with the calculated ideal response using delta function pulses.

The estimated ratios between the cascaded processes and the direct fifth-order response are in favor of the cascaded processes, even when the experimental factor in Eq. (16), using a realistic phase matching factor, is taken into account. However, the ratio is smaller than in studies not taking the local field effects into account[20] and for the $\chi^{(5)}_{llzzl'l'}$ component the ratio is close to 1. This again indicates the importance of interaction induced effects in the fifth-order response. The calculations still support the conclusion by Blank *et al.*[26] that all experiments performed earlier are dominated by the cascaded processes.

In the light of the recent experiments, that contain direct fifth-order response, it seems that the theory overestimates the intensity ratios or that the experiment overestimates the intermediate phase matching factors. The experimental factor might be connected with uncertainties concerning, for instance, the beam divergence or the sample length, which is not only determined by the sample thickness, but also by the overlap of the laser beams.[26] The estimated intermediate phase matching conditions, discriminating the fifth-order signals against the third-order cascaded response, is also not fully determined due to uncertainty in the orientation of the laser beams. On the other hand, the interaction induced effects might be calculated more accurately by including higher order terms in the multipole expansion and/or collision induced contributions.[36]

V. CONCLUSIONS

We have extended the description of the susceptibility in the finite field approach[20] by including dipole induced-dipole effects. The third-order response found using this method was shown to be in excellent agreement with the response calculated with the time correlation function method, proving the finite field method as a reliable alternative. This gives us confidence, that the finite field method can also be used to calculate the fifth-order response, where the time correlation function methods are expected to be extremely time consuming when the full MD trajectories are used.

Since the instantaneous normal mode calculations[10,11,13,42] lack the ability to describe diffusive motion, and the time correlation function response can in fifth-order only be done on very small systems,[32] the finite field method is the most promising method for further applications. This method makes it possible to provide a reasonable estimate of the relative intensity of the true fifth-order response and the competing third-order cascades.

The calculated third-order response is in excellent agreement with the experimental data, showing that the influence of many-body effects on the susceptibility is properly taken care of by including dipole induced-dipole interactions, as also suggested in several other studies.[14,15,18,20] In particular the sub-ps part of the third-order response is strongly affected by these interactions.

The shape of the calculated fifth-order response functions does not show convincing agreement with recent experiments that claimed to reveal the true fifth-order response.[27] Two possible causes for this discrepancy exist. The experiments may still be contaminated with cascaded third-order response and possibly cross terms between the cascaded response and the true fifth-order response as also suggested by the intensity ratios highly favoring the cascaded responses. The calculated intensity ratios suggest that measurement of the $\chi^{(5)}_{llzzl'l'}$ component is much more favorable for suppression of the cascaded processes than the other

components. The ratio of the two signal amplitudes for this component is four orders of magnitudes better than in the measurement of the all polarized component and two or three orders of magnitudes better than in the magic angle measurements.

Another explanation for the discrepancy between the calculated and the experimental fifth-order response could be the enhanced importance of interaction induced effects in the calculated fifth-order response. This suggests that the fifth-order response can be sensitive to collision induced effects. The short-range collision induced effects, due to the overlap of the electronic clouds, have not been included in this study. Even though this effect is not important in the third-order response, it might very well have important implications on the detailed shape important implications on the detailed shape and intensity of the fifth-order response. Work is in progress to include short-range collision effects in future simulations.[36]

APPENDIX A: THE INVERSE MOLECULAR POLARIZABILITY

The polarizability tensor elements of a linear molecule n, is given by

$$\alpha_{n,ij}=(\alpha-\tfrac{1}{3}\gamma)\delta_{ij}+\gamma x_i^n x_j^n. \tag{A1}$$

Here α is the isotropic polarizability, γ is the anisotropy, and x_i^n is the i component of the orientational unit-vector of molecule n. The tensor elements of the inverse polarizability are then given in the same form by

$$\alpha_{n,ij}^{-1}=(\varepsilon-\tfrac{1}{3}\lambda)\delta_{ij}+\lambda x_i^n x_j^n. \tag{A2}$$

Here ε is $3/(3\alpha-\gamma)$ and γ is $3/(3\alpha-2\gamma)-\varepsilon$. The relation is easily verified by matrix multiplication of the polarizability tensor and the inverse, using that the orientational vector is a unit-vector.

APPENDIX B: DERIVATIVES

The derivative of the molecular polarizability given in Appendix A with respect to a coordinate of the orientational unit-vector pointing along the molecular axis with the condition that the change is perpendicular to the molecular axis is given by

$$\left(\frac{\partial\alpha_n}{\partial x_i^n}\right)_{jk}=\gamma(x_j^n\delta_{ik}+x_k^n\delta_{ij}-2x_i^n x_j^n x_k^n). \tag{B1}$$

The derivative of the inverse molecular polarizability is found from the same expression simply by substituting γ with λ from Appendix A.

The dipole tensor between molecule n and m has the Cartesian components

$$(T_{nm})_{ij}=\frac{3\hat{r}_i\hat{r}_j-\delta_{ij}}{r^3}, \tag{B2}$$

where r is the vector from molecule m to molecule n and $\hat{r}_i$ is the i component of a unit-vector along the vector from m to n. The derivative of the dipole tensor with respect to a center-of-mass coordinate is given by

$$\left(\frac{\partial T_{nm}}{\partial r_i^n}\right)_{jk}=\frac{3}{r^7}(5r_i r_j r_k-r^2 r_i\delta_{jk}-r^2 r_j\delta_{ik}-r^2 r_k\delta_{ij}). \tag{B3}$$

[1] T. Steffen, N. A. C. M. Meinders, and K. Duppen, J. Phys. Chem. A **102**, 4312 (1998).
[2] D. McMorrow, N. Thantu, J. S. Melinger, S. K. Kim, and W. T. Lotshaw, J. Phys. Chem. A **100**, 10389 (1996).
[3] S. Ruhman, L. R. Williams, A. G. Joly, and K. A. Nelson, J. Phys. Chem. **91**, 2237 (1987).
[4] A. Waldman, U. Banin, E. Rabani, and S. Ruhman, J. Phys. Chem. **96**, 10840 (1992).
[5] Y. Tanimura and S. Mukamel, J. Chem. Phys. **99**, 9496 (1993).
[6] T. Steffen, J. T. Fourkas, and K. Duppen, J. Chem. Phys. **105**, 7364 (1996).
[7] A. Tokmakoff, M. J. Lang, X. L. Jordanides, and G. R. Fleming, Chem. Phys. **233**, 231 (1998).
[8] T. Steffen and K. Duppen, Chem. Phys. Lett. **290**, 229 (1998).
[9] T. Steffen and K. Duppen, J. Chem. Phys. **106**, 3854 (1997).
[10] R. L. Murry, J. T. Fourkas, and T. Keyes, J. Chem. Phys. **109**, 2814 (1998).
[11] S. Saito and I. Ohmine, J. Chem. Phys. **108**, 240 (1998).
[12] X. Ji, H. Alhborn, B. Space, P. B. Moore, Y. Zhou, S. Constantine, and L. D. Ziegler, J. Chem. Phys. **112**, 4186 (2000).
[13] T. Keyes and J. T. Fourkas, J. Chem. Phys. **112**, 287 (2000).
[14] L. C. Geiger and B. M. Ladanyi, J. Chem. Phys. **87**, 191 (1987).
[15] L. C. Geiger and B. M. Ladanyi, Chem. Phys. Lett. **159**, 413 (1989).
[16] B. M. Ladanyi, Chem. Phys. Lett. **121**, 351 (1985).
[17] P. A. Madden, in *Ultrafast Phenomena*, edited by D. H. Auston and K. B. Eisenthal (Springer, Berlin, 1985), Vol. IV, p. 244.
[18] K. Kiyohara, K. Kamada, and K. Ohta, J. Chem. Phys. **112**, 6338 (2000).
[19] S. Mukamel, V. Khidekel, and V. Chernyak, Phys. Rev. E **53**, R1 (1996).
[20] T. l. C. Jansen, J. G. Snijders, and K. Duppen, J. Chem. Phys. **113**, 307 (2000).
[21] W. Gadomski and B. Ratajska-Gadomska, Phys. Rev. A **34**, 1277 (1986).
[22] B. Ratajska-Gadomska and W. Gadomski, J. Chem. Phys. **108**, 8489 (1998).
[23] T. Steffen and K. Duppen, Phys. Rev. Lett. **76**, 1224 (1996).
[24] A. Tokmakoff and G. R. Fleming, J. Chem. Phys. **106**, 2569 (1997).
[25] K. Tominga and K. Yoshihara, J. Chem. Phys. **104**, 4419 (1996).
[26] D. A. Blank, L. J. Kaufman, and G. R. Fleming, J. Chem. Phys. **111**, 3105 (1999).
[27] D. A. Blank, L. J. Kaufman, and G. R. Fleming, J. Chem. Phys. **113**, 771 (2000).
[28] V. Astinov, K. J. Kubarych, C. J. Milne, and R. J. D. Miller, Opt. Lett. **25**, 853 (2000).
[29] A. Tokmakoff, J. Chem. Phys. **105**, 1 (1996).
[30] A. Tokmakoff, J. Chem. Phys. **105**, 13 (1996).
[31] S. Mukamel, *Principles of Nonlinear Optical Sepctroscopy* (Oxford University Press, New York, 1995).
[32] A. Ma and R. M. Stratt, Phys. Rev. Lett. **85**, 1004 (2000).
[33] *CRC Handbook of Chemistry and Physics*, edited by R. C. Weast (CRC Press, Boca Raton, 1983–1984).
[34] N. W. Ashcroft and N. D. Mermin, *Solid State Physics* (Saunders College, Philadelphia, 1987).
[35] J. A. C. Rullmann and P. T. v. Duijnen, Mol. Phys. **63**, 451 (1988).
[36] T. l. C. Jansen, J. G. Snijders, and K. Duppen (to be published).
[37] H. J. C. Berendsen, D. van der Spoel, and R. van Drunen, Comput. Phys. Commun. **91**, 43 (1995).
[38] H. Berendsen, J. P. M. Postma, W. F. Gunsteren, A. DiNola, and J. R. Haak, J. Chem. Phys. **81**, 3684 (1984).
[39] D. J. Tildesley and P. A. Madden, Mol. Phys. **42**, 1137 (1981).
[40] M. P. Bogaard, A. D. Buckingham, R. K. Pierens, and A. H. White, J. Chem. Soc., Faraday Trans. **74**, 3008 (1978).
[41] W. H. Press, S. A. Teukolsky, W. T. Vetterling, and B. P. Flannery, *Numerical Recipes in C*, 2nd ed. (Cambridge University Press, Cambridge, 1992).
[42] R. L. Murry, J. T. Fourkas, and T. Keyes, J. Chem. Phys. **109**, 7913 (1998).